Evidence for independent motional processes on the two interstitial sublattices of a layer-structured metal hydride: Hydrogen spin-lattice relaxation and motional narrowing in zirconium monohalide hemihydrides, $ZrXH_{0.5}$

T. Y. Hwang,* R. J. Schoenberger, D. R. Torgeson, and R. G. Barnes
Ames Laboratory and Department of Physics, Iowa State University, Ames, Iowa 50011
(Received 29 July 1982)

We report the results of a proton-magnetic-resonance investigation of hydrogen location and motion in the hemihydrides $ZrXH_{0.5}$ of the metallic layer-structured monohalides ZrX of zirconium (X=Br,Cl). Wide-line and pulsed NMR methods were employed to measure the temperature dependence of the linewidth and second moment and of the spin-lattice relaxation time in the laboratory and rotating frames. The results indicate that hydrogen forms an ordered structure on the tetrahedral (T) interstitial sublattice within the Zr metal bilayers, with some (small) random occupancy of octahedral (O) sites. Two stages of motional narrowing observed in the wide-line measurements and double minima found in the relaxation times are consistent with the occurrence of essentially independent hydrogen motional processes on the T and O interstitial sublattices. Hydrogen site occupancy probabilities, jump frequencies, activation energies for hydrogen diffusion, and conduction-electron contributions to the proton spin-lattice relaxation rate are deduced from the measurements.

I. INTRODUCTION

Recently a large number of metallic transition-metal halides have been investigated in regard to their reactions with hydrogen.[1,2] These materials represent an intermediate class of solids between conventional metals and conventional nonmetallic halides, and they have proven to be extremely interesting from the standpoint of understanding the fundamental properties of potential hydrogen-storing materials. Zirconium monochloride (ZrCl) and zirconium monobromide (ZrBr) are among the most thoroughly investigated systems, in part because they react readily and reversibly with hydrogen, and because their hydrides are very stable with respect to isothermal disproportionation into metal hydrides and more conventional metal halides.

Zirconium monohalide crystals appear as shiny black platelets, and are essentially two-dimensional metals, consisting of infinite double metal layers separated by two layers of halogen atoms. Thus the overall structure consists of infinite four-layer sheets sequenced X-Zr-Zr-X, where X represents Br or Cl. The layers and sheets are essentially cubic close-packed along the [001] directions.[3,4] A schematic view along the [110] direction of this structure is shown in Fig. 1. A strong resemblance to the transition-metal dichalcogenides (e.g., $NbSe_2$) is immediately evident. However, unlike the dichalcogenides, these monohalides readily absorb hydrogen reversibly, even at room temperature, to form the slightly nonstoichiometric phases $ZrXH_{0.5}$,[5] reported in this paper, and $ZrXH_{1.0}$. The stoichiometries and stabilities of the hydrides and the relatively small changes in x-ray powder patterns accompanying their formation are consistent with hydrogen insertion within the zirconium metal bilayers in these compounds.[2]

In the absence of single-crystal specimens of suffi-

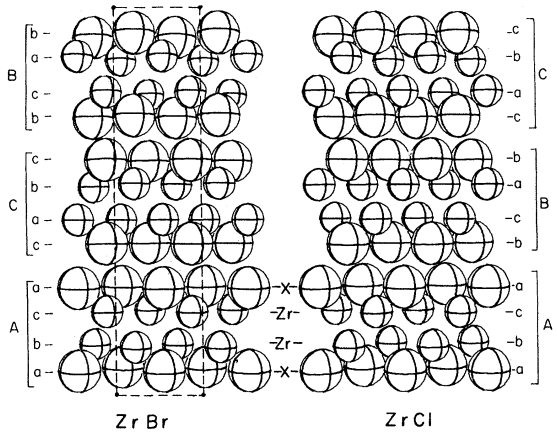

FIG. 1. Projections along [110] of the structures of ZrBr (left) and ZrCl (right). The lower-case letters refer to relative positions of close-packed layers along [001]; the capital letters to packing of the four-layer sheets.

cient dimension to permit definitive neutron structure determination, we have utilized nuclear-magnetic-resonance techniques, both steady state[6] and pulsed, to infer the probable hydrogen locations and diffusive motion in the hemihydride phases of these systems. NMR methods are particularly appropriate for these materials, first because samples are still only available as powders, and second because the zirconium nucleus ^{91}Zr has both a small natural abundance (11.2 at. %) and a small magnetic moment (1.3 nm) so that its contribution to the proton linewidth and relaxation rates is very small. Moreover, the chlorine nuclear species, ^{35}Cl and ^{37}Cl, also have small magnetic moments (0.82 and 0.68 nm, respectively) so that their contribution is also negligible. Only the bromine nuclei, ^{79}Br and ^{81}Br, have any significant effect on the proton-magnetic-resonance behavior. The net result is that the parameters characterizing the hydrogen NMR are determined almost exclusively by hydrogen-hydrogen (i.e., proton-proton) interactions and by the hydrogen motion. Measurements of the rigid-lattice second moment, of the line-narrowing behavior of the steady-state resonance, and of the spin-lattice relaxation time in both the laboratory frame (T_1) and in the rotating frame ($T_{1\rho}$) over a wide temperature range provide a large body of data from which the hydrogen locations and diffusion parameters can be inferred with considerable reliability and self-consistency.

From the measured rigid-lattice second moments M_2, the probable ordered distribution of hydrogen has been determined in the hemihydrides. We conclude that hydrogen exists interstitially *only within* the metal double layers. The metal bilayer portion of the *X*-Zr-Zr-*X* stacking sequence contains one tetrahedral (T) interstitial site and $\frac{1}{2}$ octahedral (O) interstitial site per Zr atom. The x-ray determination[5] of the structure of $ZrBrH_{0.5}$ has shown that the regular Zr polyhedra in the close-packed bilayer of ZrBr become distorted in the hemihydride as the addition of hydrogen causes a relative displacement, perpendicular to the [001] direction, between the two planes of atoms in each metal bilayer. The appearance of the resulting distorted tetrahedral and octahedral environments is seen in Fig. 2(a). The initial NMR measurements,[6] which were interpreted in terms of the original ZrBr and ZrCl structures, indicated that the hydrogen occupied alternate chains of tetrahedral sites within the metal bilayers. This conclusion lacked conviction since there appeared to be no compelling reason for such a superstructure to occur within the regular close-packed metal bilayers. However, as is clearly shown in Fig. 2(b), the chains of tetrahedral sites between the displaced metal planes in the hemihydride bring the hydrogens in adjacent chains into too close proximity and thereby provide a plausible justification for the alternate chain superstructure.

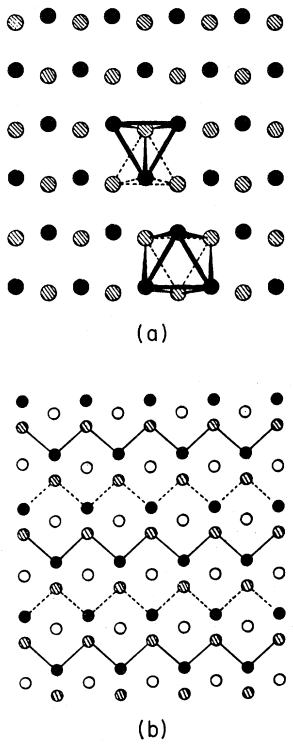

FIG. 2. Zirconium and hydrogen locations as viewed along the [001] direction (perpendicular to the metal bilayer) in $ZrBrH_{0.5}$. (a) Zirconium atoms comprising a metal bilayer. Closed circles represent Zr in one metal plane, shaded circles those in the adjacent plane below. Examples of the distorted tetrahedral and octahedral hydrogen environments are shown. (b) Hydrogen atom locations within the metal bilayer. Closed circles form one plane of tetrahedral sites, shaded circles another plane below; open circles form a plane of octahedral sites midway between. Occupied (solid lines) and empty (dashed lines) chains of tetrahedral sites are indicated.

We find that best agreement between calculated and experimental M_2 values is obtained by distributing the hydrogen over alternate chains of T sites within the metal bilayers in the hemihydride with, however, a fraction occupying the mostly empty O-site sublattice in both cases. The temperature dependence of the linewidth shows clear evidence of two stages of line narrowing.[6]

In order to clarify the mechanism of the two-stage narrowing behavior and its probable correlation with the hydrogen distribution between T and O sites, a pulsed NMR study of these systems was also undertaken, measuring T_1 and $T_{1\rho}$ over a wide temperature range. The rotating-magnetic-field (H_1) dependence of $T_{1\rho}$ was also observed.

At low temperatures the T_1 measurements show Korringa-law behavior, $T_1T=\text{const}$, confirming the assignment of hydrogen to locations within the metal bilayers. The temperature dependence of $T_{1\rho}$ shows clearly the presence of two minima, with the transition from one minimum to the other consistent with the plateau region between the two line-narrowing stages in the cw wide-line measurements. A secondary minimum is also apparent in the T_1 data. These features lead naturally to a model which incorporates independent motional processes for hydrogen on the two sublattices of interstitial T and O sites within the metal bilayers. This paper reports and summarizes all the measurements and their interpretation.

II. EXPERIMENTAL TECHNIQUES

A. Sample preparation

A detailed description of the sample preparation procedures for the zirconium monohalide hydrides has been given in Refs. 2–4. Very briefly, ZrCl and ZrBr were prepared by heating zirconium tetrahalides with zirconium turnings in a sealed tantalum tube, starting at 500 °C and increasing to about 850 °C at a rate of about 50 °C per day. The uniformity of the product was established by comparison of x-ray powder patterns. No activation of the monohalide samples was found to be necessary prior to hydrogen absorption. The initial hydrogenation rate was approximately 1 Torr/sec at 100–300 °C, using hydrogen pressures of 50–100 Torr. The oxygen contamination was estimated to be less than 0.66 wt. %. The composition measurements characterized these samples as $ZrBrH_{0.501\pm0.004}$ and $ZrClH_{0.502\pm0.004}$.

B. Wide-line measurements

The experimental arrangement utilized an induction spectrometer with crossed-coil probe[7] and signal-averaging based on a 400 channel analyzer. Variable temperatures were achieved by means of gas-flow techniques in addition to a liquid-nitrogen bath. The proton resonances were studied over the frequency range from 5 to 51 MHz and over the temperature range $77 \leq T \leq 450$ K.

C. Measurement of T_1 and $T_{1\rho}$

All relaxation-time measurements were made with a phase-coherent pulsed NMR spectrometer operated at a frequency of 37.7 MHz. The sample probe consisted of a single rf sample coil and two independently tunable rf capacitors precisely tuned so as to match the probe to the 50-Ω characteristic impedance of the interconnecting transmission lines[8] at 37.7 MHz. The digital pulse programmer[9] incorporating an auto-increment circuit[10] was utilized to generate all the pulse sequences in the experiment.

T_1 was measured using a 180°,τ,90°, free-induction-decay (FID) pulse sequence, incrementing the τ spacing between the 180° and 90° pulses. This method yielded a better signal-to-noise ratio than that obtained with a 90°,τ,90°, FID sequence which, however, yielded essentially the same results.

Signal averaging was accomplished by storing several (e.g., eight) automatically incremented T_1 recovery curves each of 100 points in the memory of a Nicolet Instrument Corporation 535 signal averager. *Each channel* location corresponded to a definite τ spacing between 180° and 90° pulses. The averaged recovery curve was fit in the least-squares sense to an exponential decay curve within a Digital Equipment Corporation LSI-11 minicomputer interfaced to the Nicolet 535. The relaxation time and quality of fit were output by the LSI-11.

The spin-lattice relaxation time in the rotating frame, $T_{1\rho}$, was measured by applying a 90° rotating pulse followed closely by a holding pulse having an rf phase 90°-advanced relative to the rotating pulse. The initial amplitude of the FID, following the holding pulse, sampled the remaining magnetization in the rotating frame.

The length of the rf locking pulse was automatically incremented by modifying the pulse programmer[9] with the addition of a 74107 JK flip-flop to channel 2. The trailing edge of the regular output (analog adjustable width) pulse of channel 2 was used to clock the 74107. The incremented[10] START pulse for channel 3 (generated in channel 2) was used to reset the flip-flop. The $\bar{Q}$ (negative true) output of the 74107 was then directed to the B phase of our two-phase rf switch.[11] This modification produced a locking pulse length which was successively incremented in digital steps.

Signal averaging of the $T_{1\rho}$ relaxation curves was accomplished and least-squares fits were made as described above for the T_1 measurements. Flux density of the holding pulses could be preset to values ranging up to 25 Oe.

A nitrogen-gas-flow technique was adapted to provide a variable sample temperature which was monitored by a copper-Constantan thermocouple near the sample. Temperature regulation was achieved by means of a current control amplifier and a heater element in the gas flow stream, with the error signal derived from the monitor thermocouple fed back to the current control amplifier. For temperatures below ambient, cold nitrogen gas was generated by boiling liquid nitrogen in a storage dewar, with temperature control also maintained as described.

III. EXPERIMENTAL RESULTS AND ANALYSIS

A. Wide-line measurements

The results of the wide-line (steady-state) measurements of the proton resonance are presented first since the second-moment data provide a principal piece of evidence supporting the alternate-chain model of hydrogen occupancy of tetrahedral (T) sites in these compounds. The line-narrowing behavior yields the activation energies for hydrogen diffusion. At high temperatures, in the fully narrowed regime, the line shape is found to be that characteristic of an axially symmetric shift tensor. These topics are taken up in order in Secs. III A 1—III A 3.

1. Rigid-lattice second moments

The experimental rigid-lattice second-moment (M_2) values for the ^{1}H resonance in the hemihydrides are listed in Table I A, where they may be compared with theoretical values calculated for several possible ordered-site distributions of the hydrogens. The calculated M_2 values are based on the x-ray structure data for $ZrBrH_{0.5}$.[5] In this case, each Zr has two metal neighbors in the adjacent layer at 3.20(3) Å and one at 3.69(5) Å, two metal neighbors in the same layer at 3.540(1) Å and four at 3.446(4) Å, and two Br neighbors on the opposite (adjacent) layer at 2.68 Å and one at 2.90 Å. The intralayer Br-Br distances are 3.45 and 3.54 Å as for Zr, while the interlayer distances are 3.71 Å. In the case of $ZrClH_{0.5}$, for which similar detailed structural data are not available, we have estimated the dimensions of the distorted interatomic spacings by scaling the change from ZrCl to $ZrClH_{0.5}$ in the same degree as in the bromide.

As has already been remarked, it appears highly probable that hydrogen enters interstitial sites within the metal bilayers. The possibility that hydrogen might occupy interstitial sites between the metal and halogen layers can be ruled out on the basis of the size of these interstitial sites. In addition, both the electronic spin-lattice relaxation time T_{1e} and the diffusion-controlled contribution T_{1d} in all of these compounds are characteristic of transition-metal—hydrogen systems, strong arguments in support of locating the hydrogen within the metal bilayers.

In Table I(a) the experimental rigid-lattice second-moment values are compared with calculated values based on three ordered-site distributions of the hydrogens in the hemihydrides. In calculating M_2 values from the Van Vleck formula,[12] account must be taken of the possible occupation of both T and O sites and of the contributions from the zirconium and halogen nuclei. These different theoretical contributions to the total M_2 are listed in Table II, assuming full occupation of T and O sites in each case. The notation M_{ij} denotes the contribution of (i) site nuclei to the second moment of a (j) site hydrogen. These summations were extended to include the fifth-nearest-neighbor hydrogens in the same metal bilayer. The notation M_{HT} and M_{HO} denotes the contribution of the host (H) lattice Zr and halogen nuclei to the second moment of hydrogen in T and O sites, respectively. These summations included the nearest-neighbor Zr and halogen atoms only.

TABLE I. (a) Experimental and theoretical rigid-lattice proton second moments in $ZrClH_{0.5}$ and $ZrBrH_{0.5}$. Several ordered hydrogen interstitial site occupation schemes are listed with corresponding calculated second-moment values. Measured values of x were used in all calculations. (b) Probability of hydrogen occupancy of octahedral interstitial sites that is required to obtain exact agreement between experimental and calculated second moments.

	$ZrClH_{0.5}$	$ZrBrH_{0.5}$
Measured hydrogen concentration x	0.502	0.501
(a)		
Second moments in $(Oe)^2$		
Experimental values ($\pm 15\%$)	4.11	4.03
Calculated values assuming:		
complete oct. site occupancy	1.68	1.50
alternate tet. site occupancy	1.71	1.58
alternate chains of tet. sites	2.82	2.52
(b)		
Probability of occupancy of octahedral sites, α	0.06	0.08

TABLE II. Calculated second-moment contributions at tetrahedral (T) and octahedral (O) sites due to protons in the T and O sublattices and to the Zr and halogen nuclei of the host (H) lattice. The notation M_{ij} means the contribution of i-site nuclei to the second moment of a j-site proton. All values are in $(\text{Oe})^2$.

	M_{TT}	M_{OT}	M_{TO}	M_{OO}	M_{HT}	M_{HO}	$M_{TT,\text{chain}}$[a]
$ZrClH_x$	10.551	14.647	29.293	1.484	0.116	0.085	2.602
$ZrBrH_x$	8.782	12.596	25.191	1.294	0.238	0.158	2.239

[a]For the zig-zag chain model, M_{TT} is reduced and M_{TO} is halved; other moments are unchanged.

We must point out here that the substantial nuclear electric quadrupole interactions of ^{91}Zr, ^{35}Cl, ^{37}Cl, ^{79}Br, and ^{81}Br which probably exist in these hexagonal lattices have been ignored in the Van Vleck second-moment formulation.[12] However, since the Zr, Cl, and Br contributions to the hydrogen M_2 are relatively minor ones, this uncertainty is not of crucial importance.

Partitioning of the second moment. The total second moment for a given assumed configuration of site occupancy can be written as[13]

$$M_2=\frac{2\beta}{2\beta+\alpha}(\beta M_{TT}+\alpha M_{OT}+M_{HT}) + \frac{\alpha}{2\beta+\alpha}(\alpha M_{OO}+\beta M_{TO}+M_{HO}) , \quad (1)$$

where α and β represent the probability of occupancy of the O and T sites, respectively, and the M_{ij}, etc., refer to the different contributions tabulated in Table II. If the hydrogen is assumed to be ordered on the tetrahedral sites, the coefficient β of M_{TT} and M_{TO} in this expression is replaced by 2β. Since there is one T site and one-half O site per metal atom within the metal bilayer, α and β are related to the hydrogen content x by

$$2\beta+\alpha=2x . \quad (2)$$

The calculated M_2 values in Table I A show that the two simplest possible orderings for the hemihydrides, namely occupation of either all O sites ($\alpha=1$, $\beta\cong 0$) or occupation of alternate T sites ($\alpha\cong 0$, $\beta\cong 0.5$), lead to essentially identical M_2 values which are less than half the experimental value. On the other hand, occupation of alternate chains of tetrahedral sites within the Zr-Zr bilayers, as shown in Fig. 2(b), leads to much closer agreement with experiment, as indicated by the calculated values appearing on the fourth line of Table I(a). It should be emphasized that the M_2 values are insensitive to the details of long-range ordering in the c direction of the structure. The arrangement of the chains in one bilayer relative to those in adjacent bilayers cannot be inferred from these measurements. Indeed, preliminary analysis of powder neutron-diffraction data suggests the absence of order between chains in different bilayers.[5]

Complete agreement between calculated and experimental M_2 values can be obtained if a small fractional occupancy of O sites occurs. The close proximity of the O and T sites gives rise to a strong contribution to M_2, as is indicated by the entries in the second and third columns of Table II. By partitioning the hydrogen between T and O sites, calculated M_2 values in agreement with experiment can be obtained, using Eq. (1) together with the known hydrogen concentration x and the measured M_2. The resultant probability of occupancy of O sites required to bring the calculated M_2 values into agreement with experiment is listed in Table I(b). Occupation of alternate chains of T sites is assumed, as described above. In $ZrClH_{0.5}$ about 6% of the hydrogen occupies O sites ($\alpha=0.06$) according to this model and in $ZrBrH_{0.5}$ an 8% occupancy is needed. This relatively small occupancy of the O sites plays an important role in the line narrowing and spin relaxation behavior in the hemihydrides, as will be seen.

2. *Line-narrowing behavior*

The temperature dependence of the linewidth in the two hemihydrides is plotted in Fig. 3. Clear evidence of the occurrence of two stages of line narrowing is seen in both compounds. The second-moment analysis (Tables I and II) leads to the conclusion that although most of the hydrogen occupies the T sublattice, a fraction enters the O sublattice. In this case, if the motion of the hydrogen occurs by independent mechanisms on the two sublattices, and if one of the mechanisms is more rapid than the other, then such two-stage narrowing is to be expected. The low-temperature stage corresponds to the fast component which has a lower on-set temperature for motional narrowing than does the slow component. This model, as demonstrated further in Sec. III B, applies also to the interpretation of the observed double $T_{1\rho}$ minimum behavior and to the secondary minimum seen in T_1.

The line-narrowing behavior has been analyzed to yield the correlation (or jump) frequency for dif-

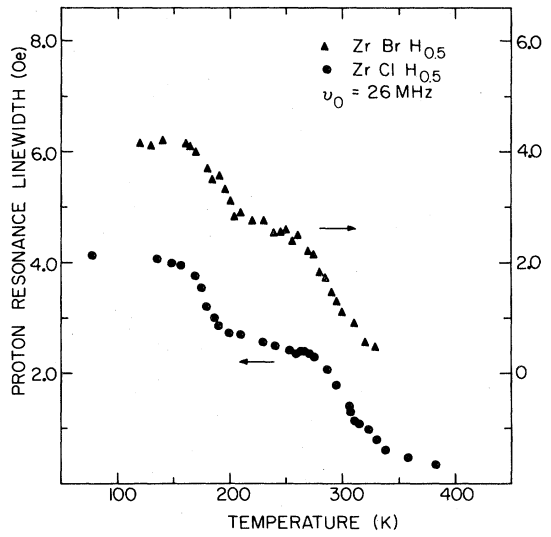

FIG. 3. Temperature dependence of the proton resonance linewidth in the hemihydride phases, $ZrClH_{0.5}$ and $ZrBrH_{0.5}$, measured at a nominal resonance frequency of 26 MHz.

fusive motion, using the empirical modification of the BPP approximation[14] suggested by Whittingham[15]

$$\nu_c = \frac{\alpha\gamma(\Delta H - \Delta H_r)}{2\pi \tan[\pi(\Delta H - \Delta H_r)^2/2(\Delta H_l - \Delta H_r)^2]}, \quad (3)$$

where ΔH is the linewidth at temperature T, ΔH_l is the low-temperature (rigid-lattice) linewidth, ΔH_r is the high-temperature, residual linewidth due to magnet inhomogeneity, γ is the nuclear gyromagnetic ratio, and α is a factor on the order of unity dependent on the line shape. In applying this analysis to the two-stage narrowing in the hemihydrides, the rigid-lattice linewidth for the high-temperature narrowing stage has been taken to be the value in the transition region ($230 \leq T \leq 270$ K).

The resulting values of the jump frequency (apart from the factor α) obtained in this manner from analysis of the $ZrClH_{0.5}$ measurements at 20 MHz are shown in Fig. 4, and the activation energies for hydrogen diffusion derived from the slopes of the lines in Fig. 4 are listed in Table III, together with the similar results for $ZrBrH_{0.5}$.

3. *High-temperature line shape*

As shown in Fig. 5, at high temperatures ($T > 400$ K) where motional narrowing of the resonance is essentially complete, the proton resonance exhibits an anisotropic shape characteristic of an axially symmetric shift tensor.[16] The observed splitting increases linearly with applied field strength, consistent with this interpretation. This anisotropy does not arise from magnet inhomogeneity.[17] In addition, it can be shown that it is not a consequence of any pronounced anisotropy in the shape of the individual particles in the samples. For these materi-

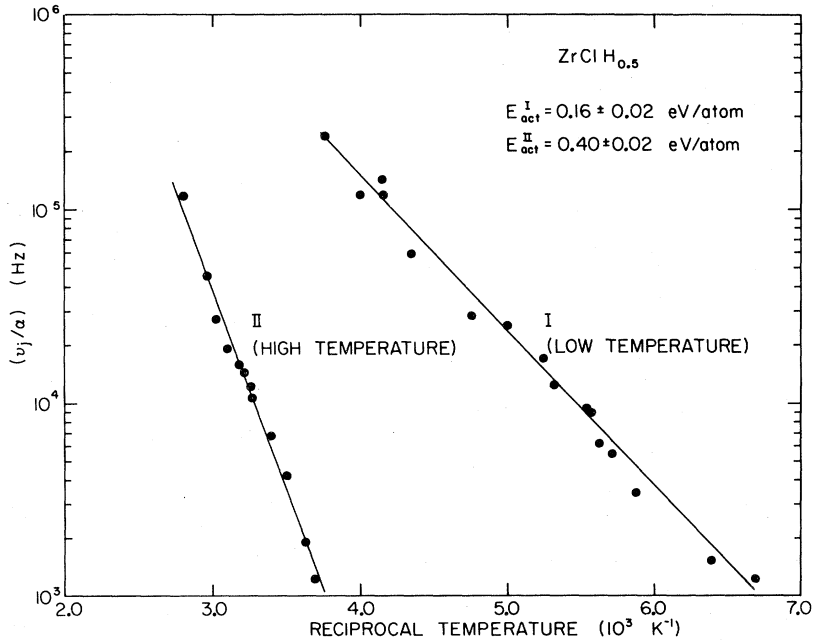

FIG. 4. Hydrogen jump frequency (correlation frequency) as a function of reciprocal temperature in $ZrClH_{0.5}$. Data points are those of Fig. 3 reduced according to Eq. (3) of the text.

TABLE III. Activation energies for hydrogen diffusion in $ZrClH_{0.5}$ and $ZrBrH_{0.5}$. The two distinct narrowing stages are specified by high temperature and low temperature, respectively.

Hydride	Measured hydrogen concentration (x)	Activation energy (eV/atom) High temp.	Low temp.
$ZrClH_{0.5}$	0.502	0.40	0.16
$ZrBrH_{0.5}$	0.501	0.45	0.17

als, which form as very thin flakes, this possibility leads to a resonance shape in which the sign of the "shift" has the opposite sign to that observed.[18] The possibility remains that the observed anisotropy is a consequence of the probable anisotropy of the bulk susceptibility of these compounds. Single-crystal susceptibility measurements are needed to resolve this question.

The measured isotropic Knight shift is very small, at the limit of our resolution, $K_{iso}=0\pm5\times10^{-4}$ %, but the anisotropic component is substantial, having the value $K_{ax}=-(2.6\pm0.2)\times10^{-3}$ % at $T>400$ K. This shift anisotropy has also been observed in $ZrClH_{0.5}$ at room temperature by means of multiple-pulse NMR to remove the static dipolar interactions which prevent its direct observation.[19] A value of $K_{ax}=-(3.4\pm0.1)\times10^{-3}$ % was obtained, suggesting that the anisotropy may be temperature dependent.

B. Relaxation-time measurements

The proton spin-lattice relaxation time T_1 and the rotating-frame spin-lattice relaxation time $T_{1\rho}$ were measured in both hemihydrides. The temperature dependence of these relaxation times was observed over a range of approximately 350 K around ambient temperature. In addition, the rf-field dependence of $T_{1\rho}$ was also measured by using two different rf-field strengths in each case. Representative experimental data are summarized in Figs. 6 and 7 for $ZrBrH_{0.5}$ and $ZrClH_{0.5}$, respectively.

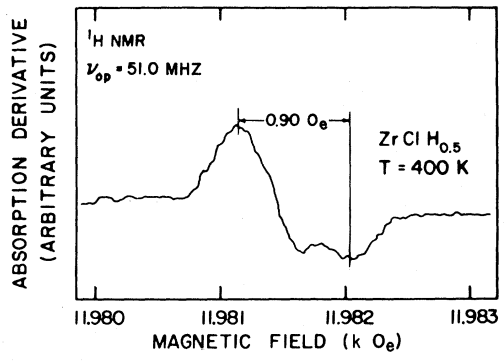

FIG. 5. Proton-magnetic-resonance line shape (absorption derivative) in $ZrClH_{0.5}$ at a temperature above the line-narrowing transition region, showing the asymmetric line-shape characteristic of Knight-shift anisotropy.

1. Conduction-electron contribution

In a metallic hydride one expects two predominant sources of proton spin-lattice relaxation: One is the electronic contribution T_{1e} due to the scalar contact interaction between spins of conduction electrons and protons, and the other, T_{1d}, results from hydrogen diffusion. The T_1 plot in Fig. 6 shows

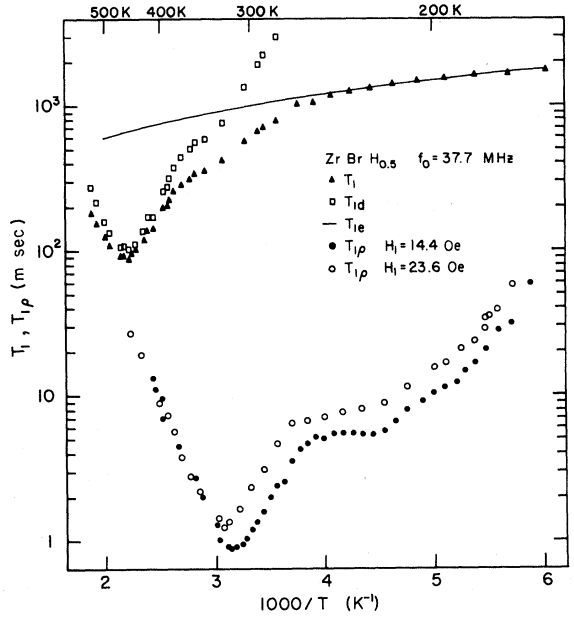

FIG. 6. Measured T_1 and $T_{1\rho}$ values for ^{1}H in $ZrBrH_{0.5}$ as a function of reciprocal temperature at a frequency of 37.7 MHz. $T_{1\rho}$ values are shown for two strengths of the rotating field H_1. Decomposition of the T_1 measurements into electronic (T_{1e}) and diffusion-controlled (T_{1d}) components is also shown. The solid curve fit to the low-temperature T_1 points represents $T_{1e}T=300$ sec K, and the resultant T_{1d} contribution is shown by the □ points.

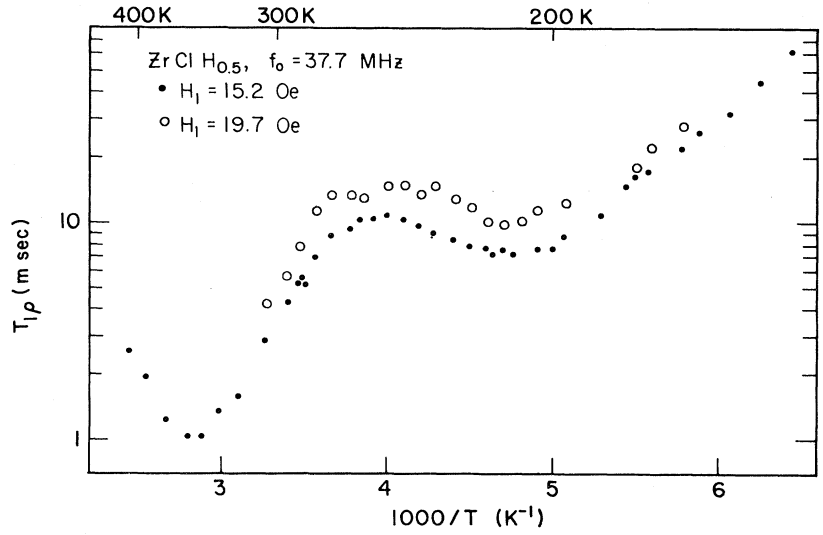

FIG. 7. Measured $T_{1\rho}$ values for ^{1}H in $ZrClH_{0.5}$ as a function of reciprocal temperature at a frequency of 37.7 MHz. Data points are shown for two strengths of the rotating field H_1.

these two contributions clearly. In the high-temperature region there is a well-defined T_1 minimum, a dominant diffusion effect. In contrast, the low-temperature T_1 data show a relatively slow variation with inverse temperature, an indication of dominant electronic relaxation. Therefore, we have

$$(T_1)^{-1}=(T_{1d})^{-1}+(T_{1e})^{-1}\ , \tag{4}$$

where the electronic contribution is characterized by the Korringa relation,[20]

$$T_{1e}T=\text{const}\ . \tag{5}$$

Applying this latter relation to the low-temperature T_1 data, the best-fit constants were found to be (in sec K): 300 for $ZrBrH_{0.5}$ and 450 for $ZrClH_{0.5}$, with probable uncertainties of about 5%. These values are very similar to those of the hydrides of the group V*B* metals, vanadium, niobium, and tantalum.

2. *Dipolar (diffusion) contribution*

The spin-lattice relaxation rate $(T_{1d})^{-1}$ of ^{1}H arising from fluctuation of the dipole interaction between both like spins I and unlike spins S (e.g., between ^{1}H and ^{91}Zr), is expressed as[21]

$$(T_{1d})^{-1}=\tfrac{3}{2}\gamma_I^4\hbar^2 I(I+1)[J^{(1)}(\omega_I)+J^{(2)}(2\omega_I)] +\gamma_I^2\gamma_S^2\hbar^2 S(S+1)[\tfrac{1}{12}J^{(0)}(\omega_I-\omega_S)+\tfrac{3}{2}J^{(1)}(\omega_I)+\tfrac{3}{4}J^{(2)}(\omega_I+\omega_S)]\ , \tag{6}$$

where $\omega_I=\gamma_I H_0$ and $\omega_S=\gamma_S H_0$ denote the Larmor frequencies of like and unlike spins, respectively. $J^{(q)}(\omega)$ is a power spectrum of the spatial correlation function of the dipolar interactions that induce changes of the total magnetic quantum number by $\Delta m=\pm q$. This expression can be simplified by assuming that the spatial correlation function is isotropic and approximately exponential with a decay constant τ_c, defined as a correlation time. Although this appears to ignore the two-dimensional nature of these compounds, the effect of the lower dimensionality on the correlation functions is expected to be significant only in the range of very short correlation times (i.e., at high temperatures).[22]

In this approximation one then obtains for powder samples[21]

$$J^{(0)}(\omega):J^{(1)}(\omega):J^{(2)}(\omega)=6:1:4\ , \tag{7}$$

$$J^{(1)}(\omega)=\tfrac{2}{15}\sum_k r_k^{-6}J(\omega,\tau_c)\ , \tag{8}$$

$$J(\omega,\tau_c)=2\tau_c/(1+\omega^2\tau_c^2)\ . \tag{9}$$

If the unlike nuclei of the host lattice are stationary, then the correlation time τ_c of the interaction between these nuclei and ^{1}H is just τ_D, the mean residence time of the hydrogen atoms in a particular interstitial site, whereas that of the ^{1}H-^{1}H interaction is $\tau_D/2$. Therefore, $(T_{1d})^{-1}$ can be expressed as

$$(T_{1d})^{-1}=\frac{4}{3}\frac{\gamma_I^2 M_{II}}{\omega_I}\left[\frac{y}{4+y^2}+\frac{y}{1+y^2}+\frac{3}{8}\sigma\left[\frac{y}{1+(1-\rho)^2y^2}+\frac{3y}{1+y^2}+\frac{6y}{1+(1+\rho)^2y^2}\right]\right], \tag{10}$$

where $y=\omega_I\tau_D$, $\rho=\omega_S/\omega_I$, and $\sigma=M_{IS}/M_{II}$. Here M_{II} and M_{IS} represent the second-moment contribution from like and unlike nuclei, respectively.

3. *Rotating frame* T_1

Following the same arguments used in arriving at Eq. (10), a similar expression can be obtained for the rotating-frame spin-lattice relaxation rate $(T_{1\rho})^{-1}$ based on the weak-collision theory approach. Under the assumptions of exact resonance and that $H_L \ll H_1 \ll H_0$, where H_L is the local field and $H_1=\omega_1/\gamma_I$ is the rotating magnetic field, one obtains approximately[23,24]

$$(T_{1\rho})^{-1}\cong\tfrac{3}{8}\gamma_I^4\hbar^2 I(I+1)J^{(0)}(2\omega_1)+\tfrac{1}{6}\gamma_I^2\gamma_S^2\hbar^2 S(S+1)J^{(0)}(\omega_1) \tag{11}$$

or

$$(T_{1\rho})^{-1}\cong\tfrac{1}{2}\gamma_I^2[M_{II}J(2\omega_1,\tau_c)+M_{IS}J(\omega_1,\tau_c)] \tag{12}$$

in the temperature region where $\omega_0\tau_c \gg 1$. As before, the first term represents the contribution from like spins with rigid-lattice second-moment M_{II}, and the second term represents the contribution from unlike spins (i.e., the spins of the host-lattice nuclei) with a second-moment contribution of M_{IS} at the I spins.

As shown in Fig. 6, the T_{1d} and $T_{1\rho}$ curves for $ZrBrH_{0.5}$ in the high-temperature region and in the vicinity of the temperature corresponding to the minimum relaxation times are consistent with the predictions of the BPP theory. The well-defined dip in the relaxation-time curves and the field dependence of the $T_{1\rho}$ curves on the long-correlation-time side of their minima indicate a relaxation mechanism dominated by atomic diffusion. However, with decreasing temperature the $T_{1\rho}$ curves reach an intermediate region extending over a temperature range of about 50 K in which they either level off or decrease somewhat before increasing again with a different slope. It is more likely that a second $T_{1\rho}$ minimum exists than that the observed behavior reflects only changes in the activation energy. The $T_{1\rho}$ curves of $ZrClH_{0.5}$, shown in Fig. 7, illustrate unambiguously this double minimum behavior in which the curves rise and fall by approximately 30% in the intermediate region before rising sharply again at low temperature. In the proton absorption linewidth measurements (Sec. III A 2) a plateaulike region was observed in the same temperature range. No similar behavior was observed in the case of the monohydrides,[6] so that this appears to be a unique feature of the hemihydrides.

C. Two-sublattice model

Assuming that the motion of hydrogen is characterized by independent processes occurring on the T and O sublattices, then it appears likely that an interpretation of the observed double-minimum behavior of the $T_{1\rho}$ data can be achieved simply by extending the conventional BPP theory to a two-sublattice system. Since the relaxation rate $(T_{1\rho})^{-1}$ is proportional to the second moment M_2, $T_{1\rho}$ can also be separated into the various contributions to M_2. If as in III A 1, the O site and T site hydrogen sublattices have probabilities of occupancy α and β and mean residence times τ_0 and τ_T, respectively, then Eq. (12) can be put in the form

$$(T_{1\rho})^{-1}=\tfrac{1}{2}\gamma_I^2\left[\frac{2\beta}{2\beta+\alpha}[2\beta M_{TT}J(2\omega_1,\tfrac{1}{2}\tau_T)+\alpha M_{OT}J(2\omega_1,\tau_D')+M_{HT}J(\omega_1,\tau_T)]+\frac{\alpha}{2\beta+\alpha}[\alpha M_{OO}J(2\omega_1,\tfrac{1}{2}\tau_0)+2\beta M_{TO}J(2\omega_1,\tau_D')+M_{HO}J(\omega_1,\tau_0)]\right], \tag{13}$$

where as before, M_{ij} denotes the second-moment contribution of i-sublattice nuclei to j-site nuclei and T, O, and H refer to T-site ^{1}H, O-site ^{1}H, and host-lattice nuclei, respectively. The coefficient 2β is used for the moments M_{TT} and M_{TO}, as occupancy of alternate zig-zag chains is assumed. The relative correlation time between T-site and O-site hydrogen, τ_D', is approximately equal to τ_0 since in the temperature range investigated, $\tau_0 \ll \tau_T$, as will become apparent. In the alternate-chain model, $M_{OT}=M_{TO}$. The linewidth analysis has indicated that $\beta \gg \alpha$ and that the M_{HO} and M_{HT} contributions are much

smaller than the other M's. In utilizing Eq. (13), therefore, the terms involving α^2 and αM_{HO} have been neglected. With these simplifications, and inserting the form of the J's one obtains

$$(T_{1\rho})^{-1}=C'\left[\left[1+\frac{\sigma_T}{\beta}\right]\frac{y_T}{1+y_T^2}+f\frac{2y_0}{1+4y_0^2}\right], \tag{14}$$

where

$$C'=2(\gamma_I^2\beta^2 M_{TT})/(2\beta+\alpha)\omega_1 ,$$

$$\sigma_T=M_{HT}/M_{TT} ,$$

and $f=\alpha M_{OT}/\beta M_{TT}$. The y's are defined by $y_T=\omega_1\tau_T$ and $y_0=\omega_1\tau_0$. The first term is the major component and dominates $(T_{1\rho})^{-1}$ in the vicinity of the deepest $T_{1\rho}$ minimum, which in the present case is the one in the high-temperature region; the presence of σ_T represents only a small correction to this term due to the ^{1}H-host nuclei interaction. The second term is the minor component, which can provide the dominant $T_{1\rho}$ mechanism only in the region far from the temperature corresponding to the major $T_{1\rho}$ minimum. This component will naturally produce a second $T_{1\rho}$ minimum value relatively greater than the value at the major $T_{1\rho}$ minimum by a factor of f. In the present case, the low-temperature $T_{1\rho}$ mechanism is dominated by this component, as shown in Figs. 7 and 8, and therefore, the corresponding minority O-site hydrogen has a shorter mean residence time than that of the majority T-site hydrogen in the temperature region investigated.

A nonlinear function-fitting procedure based on Eq. (14) was applied to one of the complete sets of $T_{1\rho}$ data for each of the hemihydrides. In Eq. (14) the C' value, which is related to the effectiveness of the relaxation mechanism, was chosen as a fitting parameter. The quantity f is proportional to α/β and involves some uncertainty in its derivation from the second moments and hydrogen concentrations, so it also was taken to be a fitting parameter. Each of the y_i incorporates two parameters, the prefactor of the jump frequency and its activation energy. Consequently a total of six parameters enter into the fitting function. The goodness of fit was justified by the mean-square deviation. The best-fit results for both $ZrBrH_{0.5}$ and $ZrClH_{0.5}$ are shown in Fig. 8 where the best-fit functions are represented by the solid curves.

The excellent agreement between the fitted functions and the $T_{1\rho}$ data for both hemihydrides over the entire temperature range indicates that this model incorporating two independent motional processes for hydrogen in the two sublattices is appropriate for these systems. The fitting functions yield the activation energies and the prefactors of the jump frequencies, $\nu_T=1/\tau_T$ and $\nu_0=1/\tau_0$, probabilities of site occupancy α and β, and the value of C', corresponding to the effectiveness of the relaxation mechanism. All of these results are listed in Table IV, together with some expected values based on the steady-state second-moment measurements of Sec. III A 1. Discussion of these results is given in Sec. IV.

As a rough check of this fitting routine, a decomposition of the data into two components was made by assuming that the relaxation rate is a simple sum

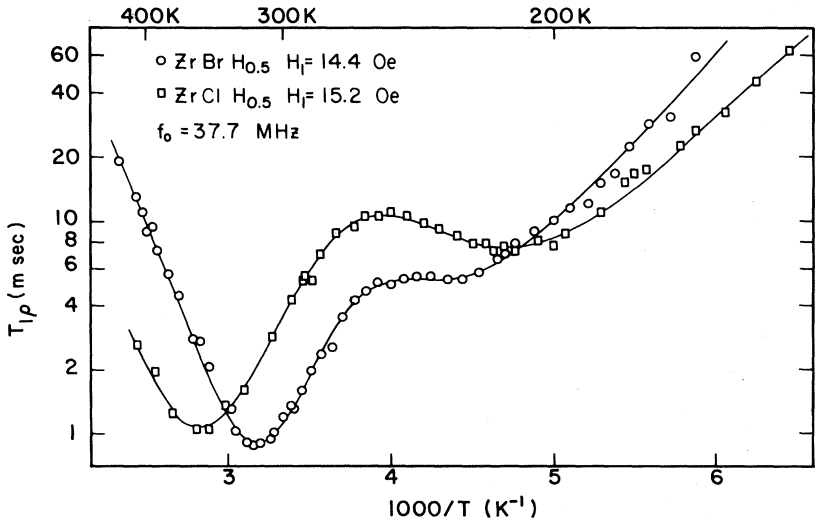

FIG. 8. Results of fitting Eq. (14) to the measured $T_{1\rho}$ values for the two hemihydrides. The data points are from Figs. 6 and 7; the solid curves are the best-fit functions.

TABLE IV. Hydrogen-jump frequency prefactors, activation energies, probabilities of occupancy α and β for tetrahedral and octahedral sublattices, and relaxation rate prefactor C', obtained from fitting rotating frame spin-lattice relaxation rate data to Eq. (14). Values for α, β, and C' based on second-moment measurements are listed after cw M_2 for comparison.

		$ZrClH_{0.5}$ ($H_1=15.2$ Oe)		$ZrBrH_{0.5}$ ($H_1=14.4$ Oe)	
		Tet. sites	Oct. sites	Tet. sites	Oct. sites
Activation energy	(eV/atom)	0.35	0.13	0.43	0.13
Jump frequency prefactor	(sec^{-1})	3.5×10^{10}	1.1×10^{9}	2.7×10^{12}	5.3×10^{8}
Probability of occupancy	$T_{1\rho}$ fit	0.49	0.02	0.49	0.02
	cw M_2	0.47	0.06	0.46	0.08
C' ($msec^{-1}$)	$T_{1\rho}$ fit	1.7		1.7	
	cw M_2	2.0		1.8	

of two power spectra of the form of Eq. (9) and that the minima in $T_{1\rho}$ are produced by one or the other of these terms. Data near the deep minimum were used to deduce an activation energy and jump-frequency prefactor for the principal component; its contribution to the relaxation rate was then subtracted from the total to determine the same parameters for the second component. This analysis yielded essentially the same values for these parameters as obtained by the nonlinear fitting procedure described above but ignores details about correlation times and yields no information about the relative strengths of the two mechanisms.

Similar indication of the occurrence of the double relaxation-time minima also appeared in the T_1 measurements on $ZrBrH_{0.5}$. By subtracting the electronic contribution from the T_1 data, a T_{1d} curve is obtained which exhibits a combination of two components as shown by the open squares in Fig. 6. However, the T_{1d} minima occur at rather closely spaced temperatures and hence their resolution is poorer than in the case of the $T_{1\rho}$ curves. Resolution is further hampered by the fact that the minor component appears in the low-temperature region where the electronic contribution to $(T_1)^{-1}$ is significant. Similar behavior was observed in the T_1 measurements on $ZrClH_{0.5}$ (not shown). However, in that case the T_{1e} contribution dominates the T_1 relaxation over all of the temperature range investigated so no analysis of T_{1d} data was made for the chloride hemihydride.

For the bromide no attempt was made to apply the detailed two-sublattice model to the T_{1d} data because of the resolution problems just mentioned and because of the complexity of the algebra involved in generalizing Eq. (10) to two sublattices. However, the simple decomposition of the relaxation rate into two terms, as described above for $T_{1\rho}$, was made and activation energies of 0.45 and 0.31 eV/atom were deduced for the high- and low-temperature mechanisms, respectively. Discussion follows in Sec. IV.

IV. DISCUSSION

A. Hydrogen locations

That hydrogen predominately occupies alternating chains of tetrahedral sites within zirconium metal bilayers is a conclusion reached from initial wide-line NMR measurements[6] and the structure of the parent compounds. The correctness of this conclusion is confirmed by the detailed analysis of the measurement of T_1 in the rotating frame ($T_{1\rho}$). In addition, the recent x-ray determination of the heavy atom structure of $ZrBrH_{0.5}$ shows that the relative displacement of adjacent metal planes produces distorted tetrahedral sites. Tetrahedral sites in adjacent chains in $ZrBrH_{0.5}$ are spaced only 2.00 Å apart, a distance generally regarded as too small for simultaneous hydrogen occupancy.[25] It should be emphasized that the NMR measurements are insensitive to the relative ordering of the hydrogen chains in different metal bilayers since even for successive bilayers the hydrogens are already too far apart to influence the proton second moment significantly. As already remarked, the preliminary analysis of powder neutron data[5] suggests the absence of order between hydrogen chains in different bilayers.

The occurrence of a chainlike superstructure for hydrogen ordering in the ZrX hemihydrides is not unique among metal-hydrogen systems. For example, as shown both by neutron diffraction[26] and NMR,[27] hydrogen (deuterium) orders in similar alternate zig-zag chains of interstitial sites to form a

superlattice at the composition $\mathscr{L}D_{2.5}$, where $\mathscr{L}$ represents La and other light lanthanides. In that case it is octahedral rather than tetrahedral sites which form the chains, the tetrahedral sites being essentially filled.

B. Electronic structure

For transition-metal hydrides the electronic contribution to the proton spin-lattice relaxation rate $(T_{1e}T)^{-1}$ may be regarded as proportional to the square of the conduction-electron density of states at the Fermi level $[N(E_F)]^2$. Accordingly, the quantity $(T_{1e}T)^{-1/2}$ furnishes an indication of the behavior of $N(E_F)$. In Fig. 9 we compare the $(T_{1e}T)^{-1/2}$ values for protons in the ZrX hemihydrides and monohydrides[28] with known values for other hydride phases of the group-IV and -V metals.[29] The magnitudes of $(T_{1e}T)^{-1/2}$ for the ZrX hydrides are seen to be entirely in accord with those of the other transition-metal hydrides. This in itself provides strong support for locating the hydrogen within the close-packed Zr layers of the structure. Of particular interest is the fact that the behavior of $(T_{1e}T)^{-1/2}$ in these hydrides tends to parallel that in the hydrides of V, Nb, and Ta, suggesting a parallel behavior of $N(E_F)$. In this connection it is worth noting that both V and Ta form hemihydride phases $VH_{0.5}$ and $TaH_{0.5}$ in parallel with ZrX.

A self-consistent band-structure calculation for ZrCl showed[30] that the Fermi level lies within the d-band complex so that the metallic properties are

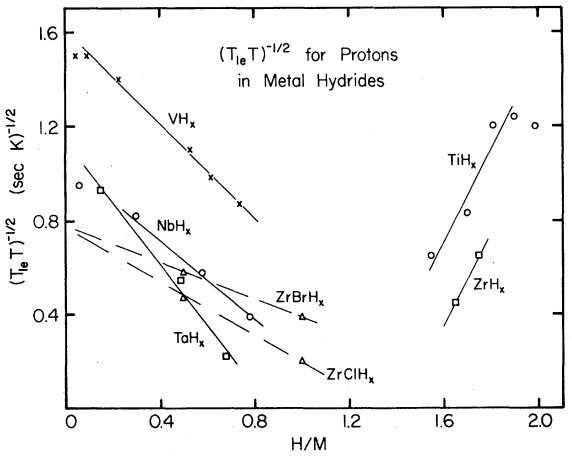

FIG. 9. Dependence of $(T_{1e}T)^{-1/2}$ on hydrogen concentration in hydrides of the group-IV and -V metals and in the ZrX hemihydrides and monohydrides. Data for ZrBrH and ZrClH are from Ref. 28; all others are from Ref. 29.

those characteristic of a d-band metal, apart form the pronounced anisotropy which results from the layer structure and the essential isolation of the metal bilayers from one another. The atomic Zr d level is about 6.5 eV higher than the Cl p level which has one hole.[30] Accordingly, the Cl p bands are easily filled by the transfer of one electron out of the Zr d states. The rest of the Zr valence electrons populate the Zr d bands to give ZrCl its d-band properties.

C. Hydrogen diffusion

Clearly, the most interesting feature of the various measurements pertaining to hydrogen motion is the strong and consistent evidence for the occurrence of two essentially independent motional processes on the two interstitial site sublattices. Successive stages of motional narrowing of the resonance shape and double (even triple) minima in the temperature dependence of T_1 are well known in the case of molecular solids.[31] In such cases substituent groups (e.g., CH_3) may rotate to cause partial line narrowing, the molecule as a whole may tumble causing further narrowing, and finally the molecules may diffuse as well. We believe, however, that the measurements reported here for the zirconium halide hemihydrides represent the first instance of such behavior for simple atomic self-diffusion. Other instances of double minima in the temperature dependence of the proton T_1 in metal hydrides have been reported and in fact interpreted in terms of independent motions on two sublattices.[32] However, recent studies have shown that such behavior can result from the presence of paramagnetic impurities in the metal lattice.[33,34] And indeed when that is the cause the two stages of motional narrowing and the double-minimum behavior of $T_{1\rho}$ are not observed. Consistent behavior of all three relaxation times (T_1, $T_{1\rho}$, and T_2) should be found and is the signature of genuine independent motional processes.

Despite the two-dimensional layering of the metal atoms in the structure of these compounds, the NMR results are consistent with three-dimensional motion of the diffusing hydrogen. Both the complete narrowing of the resonance and the absence of any frequency dependence in the $T_{1\rho}$ and T_1 behaviors on the high-temperature (short correlation time) side of the major minima in these quantities are consistent with three-dimensional motion of the hydrogen. The geometry of the zig-zag chains is such that the probable diffusion paths involve comparable components parallel and perpendicular to the metal planes even though the hydrogen remains within the metal bilayers.

To point out the three-dimensional character of the hydrogen locations, Fig. 10 shows a segment of

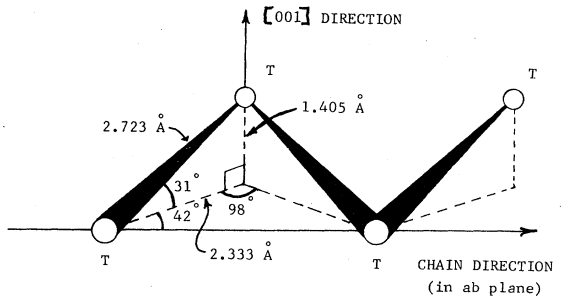

FIG. 10. Segment of a filled zig-zag chain of tetrahedral interstitial site hydrogen atoms on two planes parallel to and sandwiched between the two zirconium close-packed metal planes (not shown) which form the metal bilayer. Note the coordinate directions of the crystal relative to the zig-zag chain.

an occupied chain of tetrahedral sites. All of the tetrahedral sites lie on one or the other of two planes which are parallel to and sandwiched between the two zirconium metal planes which comprise a bilayer (see also Fig. 2). Each chain consists of sites located alternately on these two planes. The spacing of these planes of T sites is 1.4 Å in $ZrBrH_{0.5}$, as shown. This distance is an appreciable fraction of the basal plane distance of 2.3 Å between adjacent sites, also shown in Fig. 10. More importantly, the immediate neighboring site on the adjacent empty chain is also located on the opposite plane of sites (see Fig. 2) and at a distance of 2.0 Å. For motion between such sites, the jump paths contain equal in-plane and out-of-plane components.

The obvious jump paths of hydrogen among tetrahedral sites are to adjacent tetrahedral sites. The jump may be either off the occupied chain to an adjacent empty T site or to a vacancy along an otherwise filled chain of T sites. Both of these diffusive jumps require three components of motion relative to the *ab* plane and *c*-axis coordinate system of the solid. Diffusion within the zirconium bilayers is therefore three-dimensional.

In general, the diffusion jump path cannot be specified on the basis of relaxation-time measurements alone. However, in these hemihydrides, motion among all of the T sites within one bilayer will have more nearly complete three-dimensional character than motion confined to alternate chains. On this basis we infer that the second (high-temperature) stage of hydrogen motion involves motion among all tetrahedral sites and not just among T sites on the alternate filled chains occupied at low temperature.

Although the actual jump-frequency values derived from relaxation-time measurements depend on the spectral density functions employed in fitting the data,[35] values of the activation energies are relatively insensitive to such detail. We have utilized the simple Lorentzian spectral density function of the BPP formulation[14] since it clearly provides an extremely good fit to all the significant features of the data. The values of the activation energies for the T-site hydrogen derived from our measurements (Table IV) fall at the low end of those which have been obtained for the dihydrides of the group-IV metals.[36] The activation energies for the O-site hydrogen are rather small, but are about the same as the values obtained for hydrogen diffusion in the solid solution phases of the group-V metals, niobium and tantalum.[29] This similarity may be a consequence of the fact that the O-site sublattice is essentially empty as is also the case for the T-site sublattice in the solid solution phases of niobium and tantalum. The presence of the adjacent empty chains of T sites in the $ZrHM_{0.5}$ compounds may also be a factor in reducing the activation energy for the O-site hydrogen.

ACKNOWLEDGMENTS

The authors express their appreciation to Dr. A. W. Struss for the preparation of the hydride samples and to Professor J. D. Corbett and Dr. H. Marek for furnishing the results of their x-ray study prior to publication. Helpful discussions with Professors J. D. Corbett and S. H. Liu are also acknowledged. Thanks are also due Dr. R. B. Creel for critical reading of the manuscript. Dr. S. O. Nelson and R. Kroger participated in the initial stages of this work. Ames Laboratory is operated for the U.S. Department of Energy by Iowa State University under Contract No. W-7405-Eng-82. This research was supported by the Director for Energy Research, Office of Basis Energy Sciences.

*Present address: Perkin-Elmer, 2000 York Rd., Oak Brook, IL 60521.

[1]A. W. Struss and J. D. Corbett, Inorg. Chem. 17, 965 (1978).

[2]A. W. Struss and J. D. Corbett, Inorg. Chem. 16, 360 (1977).

[3]D. G. Adolphson and J. D. Corbett, Inorg. Chem. 15, 1820 (1976).

[4]R. Daake and J. D. Corbett, Inorg. Chem. 16, 2029 (1977).

[5]H. S. Marek, J. D. Corbett, and R. L. Daake, in International Symposium on the Properties and Applications

of Metal Hydrides-II, Toba, Japan, 1982 [J. Less-Common Met. (in press)].
[6]T. Y. Hwang, D. R. Torgeson, and R. G. Barnes, Phys. Lett. A 66A, 137 (1978).
[7]D. R. Torgeson, Rev. Sci. Instrum. 38, 612 (1967).
[8]I. J. Lowe and C. E. Tarr, J. Phys. E 1, 320 (1968).
[9]J. L. Conway and R. M. Cotts, Rev. Sci. Instrum. 48, 656 (1977).
[10]D. J. Adduci, P. A. Hornung, and D. R. Torgeson, Rev. Sci. Instrum. 48, 661 (1977).
[11]D. J. Adduci, P. A. Hornung, and D. R. Torgeson (unpublished).
[12]J. H. Van Vleck, Phys. Rev. 74, 1168 (1948).
[13]B. Stalinski, C. K. Coogan, and H. S. Gutowsky, J. Chem. Phys. 34, 1191 (1961).
[14]N. Bloembergen, E. M. Purcell, and R. V. Pound, Phys. Rev. 73, 979 (1948).
[15]M. S. Whittingham, in *Fast Ion Transport in Solids,* edited by W. van Gool (North-Holland, Amsterdam, 1973), p. 429.
[16]F. Borsa and R. G. Barnes, J. Phys. Chem. Solids 25, 1305 (1964).
[17]R. J. Schoenberger, R. B. Creel, B. K. Lunde, and R. G. Barnes, J. Magn. Res. 11, 20 (1973).
[18]L. E. Drain, Proc. Phys. Soc. 80, 1380 (1962).
[19]P. Dubois Murphy and B. C. Gerstein, J. Chem. Phys. 70, 4452 (1979).
[20]J. Korringa, Physica (The Hague) 16, 601 (1950).
[21]H. S. Torrey, Phys. Rev. 92, 4 (1953).
[22]P. M. Richards, in *Physics of Superionic Conductors,* edited by M. B. Salamon (Springer, New York, 1979), p. 141.
[23]D. C. Look and I. J. Lowe, J. Chem. Phys. 44, 2995 (1966).
[24]Harold T. Stokes and David C. Ailion, Phys. Rev. B 18, 141 (1978).
[25]A. C. Switendick, Int. J. Quantum Chem. 5, 959 (1971).
[26]C. G. Titcomb, A. K. Cheetham, and B. E. F. Fender, J. Phys. C 7, 2409 (1974).
[27]D. G. de Groot, R. G. Barnes, B. J. Beaudry, and D. R. Torgeson, J. Less-Common Met. 73, 233 (1980).
[28]T. Y. Hwang and M. L. S. Garcia (unpublished).
[29]For VH_x: S. Kazama and Y. Fukai, J. Phys. Soc. Jpn. 42, 119 (1977); for NbH_x: H. Lütgemeier, R. R. Arons, and H. G. Bohn, J. Magn. Res. 8, 74 (1972); for TaH_x: P. A. Hornung, A. D. Khan, D. R. Torgeson, and R. G. Barnes, Z. Phys. Chem. N.F. 116, 77 (1979); for TiH_x: C. Korn, Phys. Rev. B 17, 1707 (1978); for ZrH_x: I. A. Naskidashvili, Yu. G. Sharimanov, N. Vilcu, D. Demco, and V. Simplaceanu, Fiz. Tverd. Tela (Leningrad) 19, 3465 (1977) [Sov. Phys.—Solid State 19, 2026 (1977)].
[30]J. F. Marchiando, B. N. Harmon, and S. H. Liu, Physica 99B, 259 (1980).
[31]See, for example, P. S. Allen and A. Cowking, J. Chem. Phys. 49, 789 (1968); G. P. Jones, R. G. Eades, K. W. Terry, and J. P. Llewellyn, J. Phys. C 1, 415 (1968).
[32]See, for example, R. S. Kashaev, F. F. Gubaidullin, A. N. Gil'manov, and M. E. Kost, Fiz. Tverd. Tela (Leningrad) 22, 906 (1980) [Sov. Phys.—Solid State 22, 530 (1980)].
[33]T.-T. Phua, R. G. Barnes, D. R. Torgeson, D. T. Peterson, M. Belhoul, and G. A. Styles, in Proceedings of the International Symposium on Electronic Structure and Properties of Hydrogen in Metals, Richmond, Virginia, 1982 (Plenum, New York, in press).
[34]M. Belhoul, G. A. Styles, E. F. W. Seymour, T.-T. Phua, R. G. Barnes, D. R. Torgeson, and D. T. Peterson, J. Phys. F 12, 2455 (1982).
[35]R. M. Cotts, in *Hydrogen in Metals I. Basic Properties,* edited by G. Alefeld and J. Volkl (Springer, New York, 1978), p. 227.
[36]See, for example, J. M. Pope, P. P. Narang, and K. R. Doolan, J. Phys. Chem. Solids 42, 519 (1981).